Effects of Injection Current on the Modulation Bandwidths of Quantum-Dot Light-Emitting Diodes

Hua Xiao, Xiangtian Xiao, Dan Wu, Rui Wang, *Member, IEEE*, Kai Wang, *Member, IEEE*, and Kin Seng Chiang, *Senior Member, IEEE*

***Abstract*— This article presents an investigation of the modulation bandwidths of quantum-dot (QD) light-emitting diodes (QLEDs). The QLEDs used in our study are red-emissive CdSe/ZnS QLEDs, which have a structure of indium tin oxide (ITO)/poly(3.4-ethylene-dioxythiophene) polystyrene sulfonate (PEDOT:PSS)/TFB/QD/ZnO/Al and an emitting area of 2 or 4 mm^2. We find that at a small injection current (below ∼10 mA), the effects of the resistance–capacitance (RC) time constant and the carrier lifetime on the bandwidths of the QLEDs are comparable, while at a large injection current, the bandwidths are mainly determined by the carrier lifetime. The response time of the QDs is not a limiting factor. The bandwidths of the QLEDs increase with the injection current and are eventually limited by the damage threshold current of the devices. At the same injection current, the QLED that has a smaller emitting area provides a larger current density, and thus exhibits a larger bandwidth. At an injection current of 28 mA, the 2-mm^2 QLED provides a bandwidth of 11.4 MHz and a luminance value of 156 000 cd/m^2, and the 4-mm^2 QLED provides a bandwidth of 8.2 MHz and a luminance value of 97 000 cd/m^2. Our investigation provides a guideline for QLED-bandwidth optimization and useful information for the further development of QLEDs for lighting, display, and communication applications.**

***Index Terms*— Light-emitting diodes (LEDs), quantum dots, visible light communication (VLC).**

Manuscript received May 10, 2019; revised August 19, 2019; accepted September 11, 2019. Date of publication September 30, 2019; date of current version October 29, 2019. This work was supported in part by the National Natural Science Foundation of China under Grant 51402148, in part by Guangdong High Tech Project under Grant 2014TQ01C494, in part by the Distinguished Young Scholar of Natural Science Foundation of Guangdong under Grant 2017B030306010, and in part by Shenzhen Innovation Project under Grant JCYJ20160301113537474. The review of this article was arranged by Editor C. Surya. *(Corresponding authors: Dan Wu; Kai Wang; Rui Wang.)*

H. Xiao and K. S. Chiang are with the Department of Electrical Engineering, City University of Hong Kong, Hong Kong (e-mail: xiaocherry89@gmail.com; eeksc@cityu.edu.hk).

X. Xiao, D. Wu, and K. Wang are with the Academy for Advanced Interdisciplinary Studies, Department of Electrical and Electronic Engineering, Southern University of Science and Technology, Shenzhen 518055, China (e-mail: xiaoxt@mail.sustech.edu.cn; wud@sustech.edu.cn; wangk@sustech.edu.cn).

R. Wang is with Lab of Wireless Communications and Information System Optimization, Department of Electrical and Electronic Engineering, Southern University of Science and Technology, Shenzhen 518055, China (e-mail: wangr@sustech.edu.cn).

Color versions of one or more of the figures in this article are available online at http://ieeexplore.ieee.org.

Digital Object Identifier 10.1109/TED.2019.2941561

I. Introduction

VISIBLE light communication (VLC) has attracted much attention as a new wireless communication technology for its many unique advantages, such as immunity to electromagnetic interference, license-free operation, high security, and energy-saving [1], [2]. Light-emitting diodes (LEDs) are considered as suitable light sources for VLC [3]–[5]. Organic LEDs (OLEDs), which are widely used in mobile phone and TV screens, have been proposed for VLC [6], but their bandwidths are low (from several kilohertz to several hundred kilohertz) [7]–[10], though the micro-OLEDs with a fast response of ∼10 ns have been reported [11].

In recent years, quantum-dot (QD) LEDs (QLEDs) have emerged as promising light sources for panel display applications because of their many distinct characteristics, such as tunable emission wavelength, high efficiency, wide color gamut, and high monochromaticity [12], [13]. In comparison to common organic luminescent materials, the colloidal QDs show better performance on the response speed and color purity. Depending on the principle of light emission, the QLEDs can be divided into photoluminescence (PL)-based QLEDs and electroluminescence (EL)-based QLEDs. In a PL-based QLED, the QDs are excited optically by a conventional semiconductor LED and the emission spectra of the QDs are usually chosen to provide a balanced white light output. It is possible to use a colloidal-QD-based white LED (WLED) for VLC [14]. Using red CdSe/ZnS QDs, the bandwidth of the QD-based WLED has been increased to 2.7 MHz, while the bandwidth of a conventional phosphor-based WLED is only up to 1.55 MHz [15]. In an EL-based QLED, the QDs serve as the active medium of an LED and the light emission is achieved by injecting the electric current into the LED. To maintain balanced electron/hole injection and a high EL efficiency, the structure of an EL-based QLED is designed to consist of a hole injection layer (HIL), a hole transport layer (HTL), an emission layer, and an electron transport layer (ETL), which are usually formed with organic [16], inorganic [17], or hybrid materials [18]. In comparison to the OLEDs, the EL-based QLEDs are becoming more stable and accessible in recent years [19]. The EL-based QLEDs can be designed to generate narrow emission peaks over the entire visible light spectrum, which is particularly desirable for display applications [20].

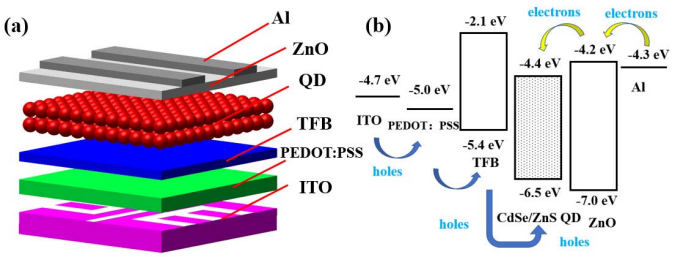

Fig. 1. (a) Schematic showing the structure of the CdSe/ZnS QLED and (b) energy level diagram showing the transport of holes and electrons across the device.

In addition to display applications, we believe that the QLEDs could also find potential applications in VLC. In general, the QDs respond faster than phosphors and, therefore, the QLEDs could offer larger modulation bandwidths than the phosphor-based WLEDs and some OLEDs. In this article, we present our results on the study of the modulation bandwidths of the EL-based QLEDs. The bandwidth of a QLED may depend on the response time of the QDs, the resistance–capacitance (*RC*) time constant of the device, and the carrier lifetime in the device. To understand the relative importance of these factors, we fabricate two batches of CdSe/ZnS QLEDs with two different emitting areas (2 and 4 mm^2) and evaluate their bandwidths. For each sample, we find that the bandwidth increases with the injection current. At the same injection current, the 2-mm^2 QLED shows a larger bandwidth than the 4-mm^2 QLED. At an injection current of 28 mA, the 2-mm^2 QLED provides a bandwidth of 11.4 MHz and a luminance value of 156 000 cd/m^2, and the 4-mm^2 QLED provides a bandwidth of 8.2 MHz and a luminance value of 97 000 cd/m^2. The highest external quantum efficiency (EQE) of the QLED achieved is 9.2%. The luminance characteristics of our QLEDs compare favorably with those of the OLEDs [21]–[23]. To our knowledge, this is the first report of the investigation of the modulation bandwidths of the QLEDs.

II. Device Fabrication and Characterization

A. Structure and Fabrication of QLEDs

Fig. 1(a) shows the structure of our QLEDs, which consists of the following layers: indium tin oxide (ITO, 100 nm)/poly(3.4-ethylene-dioxythiophene) polystyrene sulfonate (PEDOT:PSS, 40 nm)/poly (9, 9-dioctylfluorene-co-N-(4-(3-methylpropyl)) diphenylamine) (TFB, 29 nm)/CdSe/ZnS QDs (18 nm)/zinc oxide (ZnO, 33 nm)/Al (100 nm). The thicknesses of different layers were measured by a Bruker Stylus Profiler. The ITO, PEDOT:PSS, TFB, QDs, ZnO, and Al layers serve as the anode, the HIL, the HTL, the emitting layer, the ETL, and the cathode, respectively. The emitting area of the device is determined by the cross-sectional area of the Al and ITO electrodes. This typical QLED structure can achieve high stability and low threshold voltage [24]. The transport of the holes and electrons through the structure is shown in Fig. 1(b), where the values of the energy levels are taken from [25, 26]. The use of the TFB can provide a high hole mobility, and it has a lowest unoccupied molecular orbital (LUMO) (−2.1 eV) that is much higher than that of the QDs (−4.4 eV). This energy gap effectively blocks the electrons from flowing from the QDs to the anode [27]. On the other hand, the ZnO ETL serves as a blocking layer to prevent the holes from being injected from the QD layer to the Al layer. According to the transfer rule of electrons and holes in the energy bands of the semiconductors [28], the holes are injected into the QD layer through the ITO anode, the PEDOT:PSS layer, and the TFB layer from the highest occupied molecular orbital (HOMO). Meanwhile, the electrons are injected into the QD layer through the Al cathode and the ZnO layer from the conduction band. The large Coulomb force that arises from the small space of QDs forces the electrons in the LUMO and the holes in the HOMO to bond together to form electron–hole pairs as excitons. The excitons have limited lifetime and release energy in the form of light as they revert to the ground state [29].

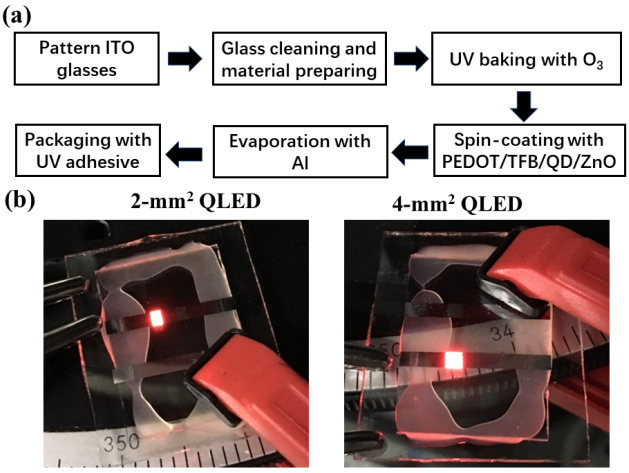

Fig. 2. (a) Steps in the fabrication process of QLED and (b) photographs of a 2- and 4-mm^2 QLED under test.

The steps in the fabrication process of the QLEDs are shown in Fig. 2(a). The electrode patterns in the form of narrow strips were first formed on an ITO glass substrate with a laser marking system. The patterned glass was cleaned in an ultrasonic bath with liquid detergent, deionized water, acetone, and isopropanol, for 10 min, respectively. After cleaning, the ITO glass was dried by nitrogen and baked in a UV-O_3 cleaning machine for 20 min. PEDOT:PSS was next spin-coated onto the cooled ITO glass at 3.5 krpm and annealed at 130 °C for 20 min. The sample was subsequently transferred to an N_2-filled glovebox. A TFB solution was spin-coated onto the sample at 3.5 krpm and baked at 120 °C for 15 min. The TFB solution was prepared by mixing the TFB powder and chlorobenzene (C_6H_5Cl) at a concentration of 10 mg/ml. A solution of CdSe/ZnS core-shell QDs (diluted to 15 mg/ml with more than 99% octane) was next spin-coated onto the sample at 3 krpm and baked at 100 °C for 5 min. A ZnO nanoparticle (20 mg/ml) film was then spin-coated onto the QD film at 3 krpm and baked at 80 °C for 10 min. Finally, the sample was transferred into a high-vacuum deposition chamber (background pressure, 4×10^{-4} Pa), where a layer of Al film cathode was deposited onto the sample to a thickness

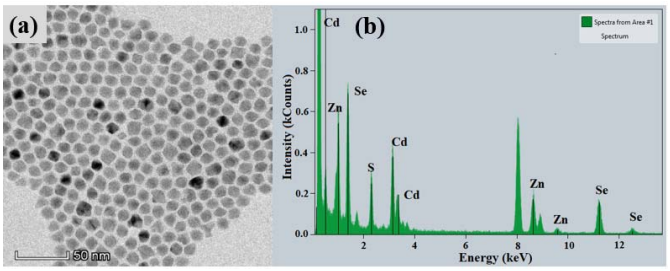

Fig. 3. (a) HRTEM image and (b) EDX analysis of the CdSe/ZnS QDs.

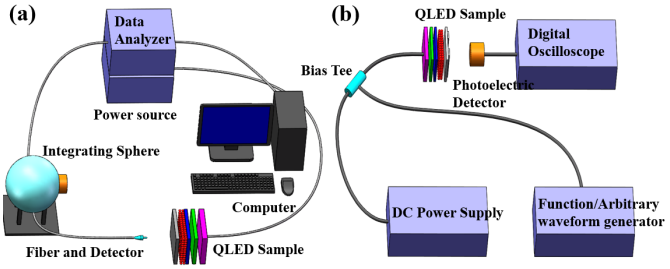

Fig. 4. Experimental setups for the measurement of (a) emission spectrum and (b) bandwidth of the QLED.

of 100 nm with a shadow mask. Two batches of QLEDs, which had emitting areas of 2 and 4 mm^2, respectively, were fabricated. Fig. 2(b) shows the photographs of a 2- and 4-mm^2 QLED under test.

B. Characterization of QDs

The red-emissive CdSe/ZnS QD solution used in our study was acquired from Mesolight Co. Ltd., Fig. 3(a) shows an image of the QDs taken by high-resolution transmission electron microscopy (HRTEM, FEI Tecnai G2 F30), which confirms that the average diameter of the QDs is 11.5 nm. Fig. 3(b) shows the result of the energy-dispersive X-ray (EDX) analysis, which confirms the elementary compositions in the QDs.

C. Optical and Bandwidth Measurement

The experimental setups for the measurement of the emission spectrum and the bandwidth of the QLED are shown in Fig. 4(a) and (b), respectively. The emission spectrum of the QLED was measured with a fiber-optic spectrometer (Ocean Optics USB 2000) through an integrating sphere and a current–luminance–voltage (J–V–L) measurement system together with a dual-channel power supply (Keithley 2614B). This system can provide direct measurements of the injection current, the luminance, and the EQE of the QLED sample. For the measurement of the modulation bandwidth, the QLED was driven with a signal that consisted of a bias dc voltage (Keysight E3641A) superimposed with a sinusoidal ac signal generated from a function/arbitrary waveform generator (RIGOL, 100 MHz, 500 MSa/s). The output light from the QLED was monitored with a photodetector (THORLABS APD120A2/M) and a digital oscilloscope (RIGOL DS4054 500 MHz 4 GSa/s). In our study, the current of the QLED

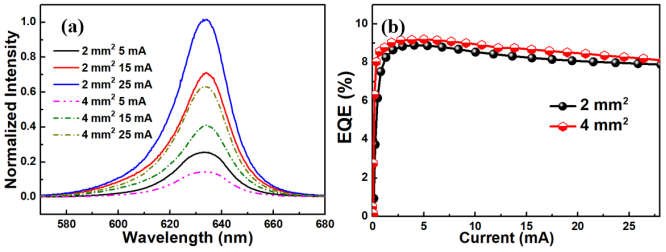

Fig. 5. (a) Normalized emission spectra of the QLED measured at various injection currents and (b) variation in the EQE of the QLED with the injection current for the 2- and 4-mm^2 QLEDs.

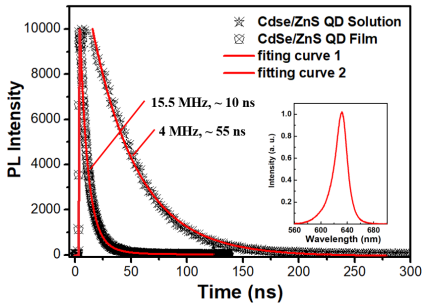

Fig. 6. Time-resolved PL spectrum for the measurement of the fluorescent lifetime of a CdSe/ZnS QD film.

was controlled by varying the dc bias voltage over the range of 2–12 V with the amplitude of the ac signal fixed at 1 V. The corresponding range of the dc injection current was 0–28 mA and the corresponding peak amplitude of the ac current was 4 mA. The 3-dB bandwidth of the QLED was determined from the measured frequency response of the output light.

III. Results and Discussion

The emission spectra of a 2- and 4-mm^2 QLED measured at different injection currents are shown in Fig. 5(a). These QLEDs provide stable emission at 634 nm with a narrow full-width-at-half-maximum (FWHM) of ~22 nm. The narrow FWHM and the stability in the emission peak guarantee pure color emission, which is important for display applications. At the same injection current, the 2-mm^2 QLED delivers more intense light, which can be attributed to the larger current density. The variation in the EQE with the injection current is shown in Fig. 5(b). The EQE of the 4-mm^2 QLED increases rapidly from 0% to a maximum value of 9.2% at a current of 1.6 mA and then decreases gradually as the current increases. The EQE of the 2-mm^2 QLED follows the same trend but is slightly lower. Similar trends have been observed with InGaN LEDs [30].

We measured the fluorescent lifetime of the QD film from the time-resolved PL spectrum using a spectrometer (Edinburgh Instruments FLS980). As shown in Fig. 6, the QD film has a fluorescent lifetime of 10 ns. We should note that the QD solution has a longer fluorescent lifetime of 55 ns. The faster response of the QD film is due to an increase in the nonradiative decay rate as the QD molecules are aggregated within the film [31], [32]. The fluorescence spectrum of the QD film is also shown in the inset of Fig. 6. The peak

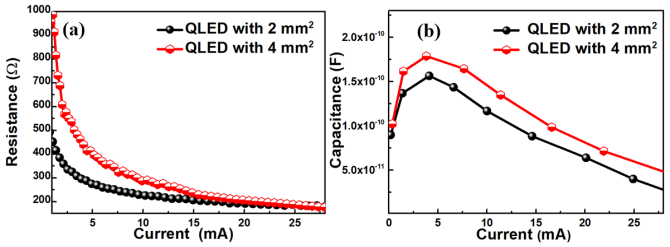

Fig. 7. Variations in (a) resistance and (b) capacitance values with the injection current measured for the 2- and 4-mm^2 QLEDs.

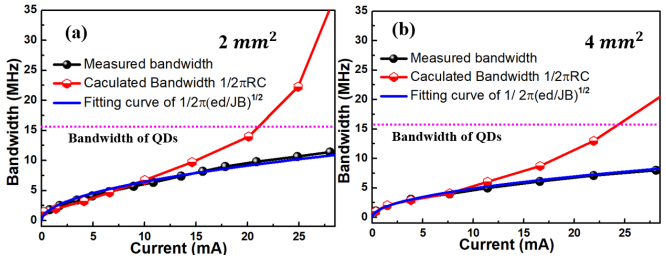

Fig. 8. Variations in the measured bandwidth and the bandwidth calculated from the *RC* time constant with the injection current for (a) 2-mm^2 QLED and (b) 4-mm^2 QLED.

wavelength of the fluorescence spectrum is shorter than that of the EL spectra shown in Fig. 5(a) by ∼3 nm, which is due to the Förster resonant energy transfer from smaller (donor) to larger (acceptor) dots within the QDs [33]. Our results confirm that the emission peaks of the CdSe QDs under photoluminescent and EL conditions are close [34].

The relationship between the response time τ and the modulation bandwidth f is given by $f = 1/(2\pi\tau)$. If the bandwidth of the QLED was limited by the fluorescent lifetime of the QD film, with $\tau = 10$ ns, the theoretical and measured bandwidth are 15.9 and 15.5 MHz, respectively. The *RC* time constant should also affect the bandwidth of a QLED [35]. To obtain the R and C values of the QLED, we measured the current–voltage and capacitance–voltage relationships of the QLED with a semiconductor parameter analyzer (Keithley 4200A-SCS, 50 kHz). The variations in the R and C values with the injection current for the 2- and 4-mm^2 QLEDs are shown in Fig. 7(a) and (b), respectively. At the same current, the R and C values of the 2-mm^2 QLED are smaller than those of the 4-mm^2 QLED. The resistivity coefficient ρ can be expressed as [36]

$$\rho = \frac{\rho_0}{\kappa(1 - In\kappa)} \tag{1}$$

with

$$\rho_0 = \frac{mv_F}{ne^2 l_{\text{bulk}}} \tag{2}$$

where ρ_0 is the bulk resistivity, κ is a thickness-dependent parameter, n is the electron concentration, v_F is the Fermi velocity, e is the electron charge, m is the effective mass of electron, and l_{bulk} is the bulk mean free path. As the bulk resistivity is inversely proportional to the electron concentration, which is proportional to the current density, the resistance of the device decreases with an increase in the current. The total capacitance of a QLED is given by $C = C_D + C_R$, where C_D is the diffusion capacitance and C_R is the radiative-recombination-based capacitance [37]. An increase in the current causes a decrease in the radiative-recombination-based capacitance, which thus leads to a reduction in the total capacitance. Knowing the R and C values of the QLED, we can estimate the *RC*-limited bandwidth by $f = 1/(2\pi RC)$.

We measured the bandwidths of both the 2- and 4-mm^2 QLEDs at various injection currents and compared the results calculated by the *RC* time constants. The results are shown in Fig. 8. For both QLEDs, at a small current, the *RC*-limited bandwidth agrees with the measured bandwidth of the QLED. As the current becomes sufficiently large (∼10 mA), the *RC*-limited bandwidth becomes larger than the measured bandwidth and the discrepancy increases rapidly with the current. These results indicate that the bandwidth of the QLED is not only limited by the *RC* time constant. The measured bandwidth is also much smaller than ∼15.5 MHz, that is, the bandwidth of the QD film, which suggests that the bandwidth of the QLED is not limited by the response time of QDs. The remaining factor that affects the bandwidth of a QLED is the carrier lifetime τ_c, which is given by Zhang *et al.* [33]

$$\tau_c = \left(\frac{ed}{JB}\right)^{1/2} \tag{3}$$

where d is the thickness of the QD layer, J is the current density, and B is the recombination constant. From (3), we known the bandwidth f has a direct relationship with J and B. With the experimental obtained values of J under various currents, and the already known values of e and d, we fit the measured bandwidth (the black curve in Fig. 8) and obtain the fitting curve (the blue curve in Fig. 8). Our fitting curves match well with the experimental results both for the 2- and 4-mm^2 QLEDs, indicating the bandwidth of the QLED is mainly limited by the carrier lifetime at large currents. The values of B in (3) are obtained as 0.95×10^{-10} and 1.15×10^{-10} cm^{3}s^{-1} for the 2- and 4-mm^2 QLEDs, respectively, which agree well with the theoretical ones, such as 10^{-10} cm^3 s^{-1} given in [38] and 1.1×10^{-10} cm^3 s^{-1} given in [39]. The smaller B of the 2-mm^2 QLED is due to its larger perimeter/area ratio, which leads to a higher probability of current leakage [40], and hence, less effective recombination (i.e., a smaller B value). The fact that the bandwidth–current relationship fits very well the expression $f = 1/(2\pi\tau_c)$, as shown in Fig. 8, confirms that the bandwidth of the QLED is mainly limited by the carrier lifetime above 10 mA.

According to (3), the carrier lifetime decreases with the thickness of the QD layer. In our study, the thickness of the QD layer is 18 nm, which is close to the QD diameter (∼12 nm). There is not much room to further decrease the carrier lifetime by decreasing the thickness of the QD layer. As the thickness of the QD layer is small, compared with the thickness of the whole device, the *RC* time constant depends only weakly on the thickness of the QD layer. The response time of the QDs, which is an intrinsic property of the QDs, should not depend on the structure of the QLED.

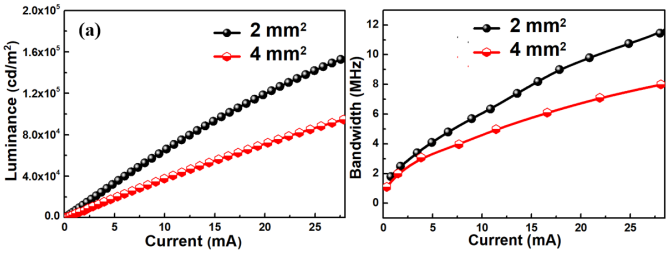

Fig. 9. Comparison of (a) luminance and (b) bandwidth characteristics of the 2- and 4-mm^2 QLEDs.

We should note that the bandwidth of a conventional GaN LED chip is limited by the *RC* time constant when the junction area is larger than 200×200 μm^2 [41]. The carrier lifetime in a GaN LED is typically several nanoseconds [42], which is shorter than that in a QLED ($\sim$10 ns).

The variations in the luminance and the bandwidth with the injection current for the 2- and 4-mm^2 QLEDs are shown in Fig. 9(a) and (b), respectively. Our results show that at the same injection current, the luminance and the bandwidth of the 2-mm^2 QLED are larger than those of the 4-mm^2 QLED. This is because the 2-mm^2 QLED provides larger current density than that of the 4-mm^2 QLED under the same current, and therefore provide shorter τ_c and higher bandwidth. The idea of increasing the bandwidth of an LED by reducing its emitting area has been proposed [43]. Our study of QLEDs concurs with this proposal.

As shown in Fig. 9, at an injection current of 28 mA, which is close to the damage threshold currents of our fabricated devices, the 2-mm^2 QLED provides a bandwidth of 11.4 MHz and a luminance value of 156 000 cd/m^2, and the 4-mm^2 QLED provides a bandwidth of 8.2 MHz and a luminance value of 97 000 cd/m^2.

IV. Conclusion

We have studied the effects of the injection current on the modulation bandwidths of the QLEDs that have different emitting areas. Our experimental results and analysis for the 2- and 4-mm^2 QLEDs confirm that at an injection current below $\sim$10 mA, the *RC* time constant and the carrier lifetime have comparable effects on the bandwidths of the QLEDs, while at a larger injection current, it is mainly the carrier lifetime that determines the bandwidths. The response time of the QDs is not a limiting factor. The bandwidths of the QLEDs increase with the injection current and are limited by the damage threshold current. At the same injection current, the luminance and the bandwidth of the QLED that has a smaller emitting area are larger than those of the QLED that has a larger emitting area. At an injection current of 28 mA, which is close to the damage threshold currents of our fabricated devices, the 2-mm^2 QLED provides a bandwidth of 11.4 MHz and a luminance value of 156 000 cd/m^2, and the 4-mm^2 QLED provides a bandwidth of 8.2 MHz and a luminance value of 97 000 cd/m^2. The highest EQE achieved is 9.2%. Our results should be useful for the development of QLEDs for lighting, display, and communication applications.

References

[1] H. Zhang, A. Yang, L. Feng, and P. Guo, "Gb/s real-time visible light communication system based on white LEDs using T-bridge cascaded pre-equalization circuit," *IEEE Photon. J.*, vol. 10, no. 2, Apr. 2018, Art. no. 7901807.

[2] H. Li, X. Chen, J. Guo, Z. Gao, and H. Chen, "An analog modulator for 460 Mb/s visible light data transmission based on OOK-NRS modulation," *IEEE Wireless Commun.*, vol. 22, no. 2, pp. 68–73, Apr. 2015.

[3] C. Wang, Y.-Y. Yu, Y.-J. Zhu, T. Wang, and Y.-W. Ji, "Multi-LED parallel transmission for long distance underwater VLC system with one SPAD receiver," *Optics Commun.*, vol. 410, nos. 889–895, Mar. 2018.

[4] H. Li *et al.*, "682 Mbit/s phosphorescent white LED visible light communications utilizing analog equalized 16QAM-OFDM modulation without blue filter," *Opt. Commun.*, vol. 354, pp. 107–111, Nov. 2015.

[5] C.-W. Hsu, C.-W. Chow, I.-C. Lu, Y.-L. Liu, C.-H. Yeh, and Y. Liu, "High speed imaging 3×3 MIMO phosphor white-light LED based visible light communication system," *IEEE Photon. J.*, vol. 8, no. 6, Dec. 2016, Art. no. 7907406.

[6] P. A. Haigh, Z. Ghassemlooy, S. Rajbhandari, and I. Papakonstantinou, "Visible light communications using organic light emitting diodes," *IEEE Commun. Mag.*, vol. 51, no. 8, pp. 148–154, Aug. 2013.

[7] P. Q. Thai, "Real-time 138-kb/s transmission using OLED with 7-kHz modulation bandwidth," *IEEE Photon. Technol. Lett.*, vol. 27, no. 24, pp. 2571–2574, Dec. 2015.

[8] P. A. Haigh, Z. Ghassemlooy, I. Papakonstantinou, and H. L. Minh, "2.7 Mb/s with a 93-kHz white organic light emitting diode and real time ANN equalizer," *IEEE Photon. Technol. Lett.*, vol. 25, no. 17, pp. 1687–1690, Sep. 2013.

[9] P. A. Haigh *et al.*, "A 1-Mb/s visible light communications link with low bandwidth organic components," *IEEE Photon. Technol. Lett.*, vol. 26, no. 13, pp. 1295–1298, Jul. 2014.

[10] H. Chun, C. J. Chiang, A. Monkman, and D. O'Brien, "A study of illumination and communication using organic light emitting diodes," *J. Lightw. Technol.*, vol. 31, no. 22, pp. 3511–3517, Nov. 15, 2013.

[11] L. Zeng *et al.*, "Electrical and optical impulse response of high-speed micro-OLEDs Under ultrashort pulse excitation," *IEEE Trans. Electron Devices*, vol. 64, no. 7, pp. 2942–2948, Jul. 2017.

[12] R. Vasan, H. Salman, and M. O. Manasreh, "Solution processed high efficiency quantum dot light emitting diode with inorganic charge transport layers," *IEEE Electron Device Lett.*, vol. 39, no. 4, pp. 536–539, Apr. 2018.

[13] D. Kim *et al.*, "Improved electroluminescence of quantum dot light-emitting diodes enabled by a partial ligand exchange with benzenethiol," *Nanotechnology*, vol. 27, no. 24, Art. no. 245203, Mar. 2016.

[14] N. Laurand *et al.*, "Hybrid organic/inorganic nanocrystal-based composite for color-conversion and visible light communications," in *Proc. 23rd Annu. Meeting IEEE Photon. Soc.*, Nov. 2010, pp. 150–151.

[15] X. Xiao *et al.*, "Improving the modulation bandwidth of LED by CdSe/ZnS quantum dots for visible light communication," *Opt. Express*, vol. 24, no. 19, pp. 21577–21586, Sep. 2016.

[16] T. Ding *et al.*, "Improved quantum dot light-emitting diodes with a cathode interfacial layer," *Organic Electron.*, vol. 32, pp. 89–93, May 2016.

[17] X. L. Zhang, H. T. Dai, J. L. Zhao, C. Li, and S. G. Wang, "Effects of the thickness of NiO hole transport layer on the performance of all-inorganic quantum dot light emitting diode," *Thin Solid Films*, vol. 567, pp. 72–76, Sep. 2014.

[18] M.-M. Yan *et al.*, "Enhancing the performance of blue quantum-dot light-emitting diodes based on Mg-doped ZnO as an electron transport layer," *IEEE Photon. J.*, vol. 9, no. 2, Apr. 2017, Art. no. 8200508,

[19] H. C. Wang *et al.*, "Cadmium-Free InP/ZnSeS/ZnS heterostructure-based quantum dot light-emitting diodes with a ZnMgO electron transport layer and a brightness of Over 10 000 cd m^{-2}," *Small*, vol. 13, no. 13, Jan. 2017, Art. no. 1603962.

[20] C.-F. Lai, Y.-C. Tien, H.-C. Tong, C.-Z. Zhong, and Y.-C. Lee, "High-performance quantum dot light-emitting diodes using chip-scale package structures with high reliability and wide color gamut for backlight displays," *RSC Adv.*, vol. 8, no. 63, pp. 35966–35972, Oct. 2018.

[21] W.-C. Chen, Y. Yuan, Z.-L. Zhu, Z.-Q. Jiang, L.-S. Liao, and C.-S. Lee, "Polyphenylnaphthalene as a novel building block for high-performance deep-blue organic light-emitting devices," *Adv. Opt. Mater.*, vol. 6, no. 2, Dec. 2018, Art. no. 1700855.

[22] Y. Wang *et al.*, "High-efficiency red organic light-emitting diodes based on a double-emissive layer with an external quantum efficiency over 30%," *J. Mater. Chem. C*, vol. 6, no. 26, pp. 7042–7045, Jun. 2018.

[23] H. Fukagawa *et al.*, "Long-lived flexible displays employing efficient and stable inverted organic light-emitting diodes," *Adv. Mater.*, vol. 30, no. 28, May 2018, Art. no. 1706768.
[24] H. Shen *et al.*, "Efficient and bright colloidal quantum dot light-emitting diodes via controlling the shell thickness of quantum dots," *ACS Appl. Mater. Inter.*, vol. 5, no. 22, pp. 12011–12016, Nov. 2013.
[25] Y. Shang and Z. Ning, "Colloidal quantum-dots surface and device structure engineering for high-performance light-emitting diodes," *Nat. Sci. Rev.*, vol. 4, no. 2, pp. 170–183, Mar. 2017.
[26] J. Chen *et al.*, "All solution-processed stable white quantum dot light-emitting diodes with hybrid ZnO TiO_2 as blue emitters," *Sci. Rep.*, vol. 4, p. 4085, Feb. 2014.
[27] K.-S. Cho *et al.*, "High-performance crosslinked colloidal quantum-dot light-emitting diodes," *Nature Photon.*, vol. 3, no. 6, pp. 341–345, May 2009.
[28] J. H. Kim, D. R. Lee, S. H. Han, and J. Y. Lee, "Over 20% external quantum efficiency in red thermally activated delayed fluorescence organic light-emitting diodes using a reverse intersystem crossing activating host," *J. Mater. Chem. C*, vol. 6, no. 20, pp. 5363–5368, Apr. 2018.
[29] G. J. Supran *et al.*, "QLEDs for displays and solid-state lighting," *MRS Bull.*, vol. 38, no. 9, pp. 703–711, 2013.
[30] L. B. Chang, M. J. Lai, R.-M. Lin, and C.-H. Huang, "Effect of electron leakage on efficiency droop in wide-well InGaN-based light-emitting diodes," *Appl. Phys. Express*, vol. 4, no. 1, pp. 481–493, Jan. 2011.
[31] A. K. Bansal *et al.*, "Photophysical and structural characterisation of in situ formed quantum dots," *Phys. Chem. Chem. Phys.*, vol. 16, no. 20, pp. 9556–9564, Apr. 2014.
[32] F. Zhang *et al.*, "Super color purity green quantum dot light-emitting diodes fabricated by using CdSe/CdS nanoplatelets," *Nanoscale*, vol. 8, no. 24, pp. 12182–12188, May 2016.
[33] X. Zhang, H. Dai, J. Zhao, S. Wang, and X. Sun, "All-solution processed composite hole transport layer for quantum dot light emitting diode," *Thin Solid Films*, vol. 603, pp. 187–192, Mar. 2016.
[34] B. O. Dabbousi and M. G. Bawendi, "Electroluminescence from CdSe quantum-dot/polymer composites," *Appl. Phys. Lett.*, vol. 66, no. 11, pp. 1316–1318, Mar. 1995.
[35] J. J. D. McKendry *et al.*, "High-speed visible light communications using individual pixels in a micro light-emitting diode array," *IEEE Photon. Technol. Lett.*, vol. 22, pp. 1346–1348, Sep. 15, 2010.
[36] F. Lacy, "Developing a theoretical relationship between electrical resistivity, temperature, and film thickness for conductors," *Nanosc. Res. Lett.*, vol. 6, no. 1, p. 636, Dec. 2011.
[37] C. Y. Zhu *et al.*, "Negative capacitance in light-emitting devices," *Solid-State Electron.*, vol. 53, no. 3, pp. 324–328, Feb. 2009.
[38] R. H. Saul, "Recent advances in the performance and reliability of InGaAsP LED's for lightwave communication systems," *IEEE Trans. Electron Devices*, vol. ED-30, no. 4, pp. 285–295, Apr. 1983.
[39] K. Ikeda, S. Horiuchi, T. Tanaka, and W. Susaki, "Design parameters of frequency response of GaAsâĽ"(Ga,Al)As double heterostructure LED's for optical communications," *IEEE Trans. Electron Devices*, vol. ED-24, no. 7, pp. 1001–1005, Jul. 1977.
[40] D. S. Meyaard *et al.*, "On the temperature dependence of electron leakage from the active region of GaInN/GaN light-emitting diodes," *Appl. Phys. Lett.*, vol. 99, no. 4, Jul. 2011, Art. no. 041112.
[41] Z. Zhou, B. Yan, X. Ma, D. Teng, L. Liu, and G. Wang, "GaN-based mid-power flip-chip light-emitting diode with high -3 dB bandwidth for visible light communications," *Appl. Opt.*, vol. 57, no. 11, pp. 2773–2778, Apr. 2018.
[42] J. S. Im, A. Moritz, F. Steuber, V. Härle, F. Scholz, and A. Hangleiter, "Radiative carrier lifetime, momentum matrix element, and hole effective mass in GaN," *Appl. Phys. Lett.*, vol. 70, no. 5, pp. 631–633, Jan. 1997.
[43] R. X. G. Ferreira *et al.*, "High bandwidth GaN-based micro-LEDs for multi-Gb/s visible light communications," *IEEE Photon. Technol. Lett.*, vol. 28, no. 19, pp. 2023–2026, Oct. 2016.